Hydrological Sciences Journal

ISSN: 0262-6667 (Print) 2150-3435 (Online) Journal homepage: https://www.tandfonline.com/loi/thsj20

Investigating hydrogeomorphic floodplain mapping performance with varying DTM resolution and stream order

A. Annis, F. Nardi, R. R. Morrison & F. Castelli

To cite this article: A. Annis, F. Nardi, R. R. Morrison & F. Castelli (2019) Investigating hydrogeomorphic floodplain mapping performance with varying DTM resolution and stream order, Hydrological Sciences Journal, 64:5, 525-538, DOI: 10.1080/02626667.2019.1591623

To link to this article: https://doi.org/10.1080/02626667.2019.1591623

Accepted author version posted online: 07 Mar 2019.
Published online: 02 Apr 2019.

HYDROLOGICAL SCIENCES JOURNAL
2019, VOL. 64, NO. 5, 525–538
https://doi.org/10.1080/02626667.2019.1591623

Investigating hydrogeomorphic floodplain mapping performance with varying DTM resolution and stream order

A. Annis [a,b], F. Nardi [a], R. R. Morrison [c] and F. Castelli [b]

[a]Water Resource Research and Documentation Centre (WARREDOC), Università per Stranieri di Perugia, Perugia, Italy; [b]DICEA, University of Florence, Florence, Italy; [c]Department of Civil and Environmental Engineering, Colorado State University, Fort Collins, Colorado, USA

ABSTRACT

Hydrogeomorphic models allow parsimonious, fast and effective floodplain extent mapping using topographic data as the main input. Hydrogeomorphic approaches enforce the principle that floodplains are well-distinguished and unique landscape features within river corridors. We investigated the sensitivity of a hydrogeomorphic floodplain delineation algorithm, based on a hydrological power law, relating flow depth to contributing area, digital terrain model (DTM) resolution and river network hierarchy. In addition, we compared the results to other common floodplain mapping methods using standard flood-hazard maps as a reference. Taking the Arno River Basin, Italy, as a case study, our results show a dependency between the optimal power law parameters and DTM resolution, with larger parameter values required to reach optimal consistency with flood-hazard maps as DTM resolution increased. Floodplain mapping performance was also found to depend on stream order. We further tested the model consistency at a larger scale to evaluate its performance with respect to inundation maps in Hungary, Italy, Spain and the UK. Our study suggests that pre-defined power law parameters can be assumed, considering DTM resolution and stream order, supporting the use of the presented hydrogeomorphic model for large-scale floodplain mapping in ungauged basins where reference flood-hazard maps are not available.

ARTICLE HISTORY
Received 22 March 2018
Accepted 19 January 2019

EDITOR
A. Castellarin

ASSOCIATE EDITOR
R. Van Nooijen

KEYWORDS
floodplain; DTM resolution; stream order; hydrogeomorphic model; terrain analysis; scaling laws

1 Introduction

As flooding risk increases around the world, techniques for identifying floodplains at large spatial scales are becoming more important (Di Baldassarre *et al.* 2010). Human growth in riverine environments is creating unprecedented stresses on water management activities, as well as disrupting hydrological functions and ecological connectivity of river–floodplain systems (Bradshaw *et al.* 2007, Scheel *et al.* 2018). Damages and fatalities connected to floods are impacting on the safety and wellness of the world population regardless of climatic and socio-economic conditions (EM-DAT 2013, Montanari *et al.* 2013, Ignacio *et al.* 2015, Nardi *et al.* 2018a). Fast, efficient techniques for mapping flood inundation areas, especially in ungauged regions of the world, can help populations prepare for and mitigate flood risks. Given the increasing availability of Earth observation datasets and computational efficiency, it is an opportune time to develop and evaluate global floodplain mapping models.

Numerous floodplain mapping techniques have been developed in recent times that generally rely on hydrological and hydraulic models. Alfieri *et al.* (2014) presented a cascade of distributed hydrological and hydraulic models at the pan-European scale for producing a 100-m resolution flood map. Sampson *et al.* (2015), Alfieri *et al.* (2017) and Dottori *et al.* (2016a, 2016b)) performed global hazard flood mapping at different resolutions: ~90 m for Sampson *et al.* (2015), and ~1 km for Alfieri *et al.* (2017) and Dottori *et al.* (2016a), 2016b), using hydrological and hydraulic modelling. Most recently, Wing *et al.* (2017) developed a 30-m resolution, two-dimensional hydrodynamic model of the USA using only publicly available data. Hydrodynamic models represent the most comprehensive method for flood-hazard analysis, providing detailed event-based inundation simulations with associated fundamental variables, such as maximum flow depth, velocity and volume. These models account for the effects of human-made obstacles and structures e.g. (bridges, weirs and levees), simulating backwater effects, flood wave attenuation and complex flood-water interactions in urban areas. Although the feasibility and efficiency of large- to global-scale hydraulic floodplain mapping models is increasing, as more detailed topographic data become available and computational processing power increases, there are

CONTACT A. Annis antonio.annis@unistrapg.it

still major challenges and issues to solve. Uncertainty of boundary conditions for inundation models, limitations in knowledge of river profile and roughness, and proper consideration of the presence of anthropogenic features, such as dikes and levees, in hydraulic systems suggest that large-scale hydrodynamic models are still difficult to replicate, even for advanced flood modellers (Ward *et al.* 2015).

Hydrogeomorphic models represent a different paradigm of floodplain mapping using topographic datasets of fluvial corridors. Hydrogeomorphic approaches enforce the principle that floodplains are well-distinguished landscape features and can be recognized for their unique morphology with respect to surrounding hill slopes (Baynes *et al.* 2015, Dietrich and Perron 2006, Nardi *et al.* 2006). River valleys are separated by uplands following well-defined breaks in slope that are clearly distinguishable in digital terrain models (DTMs), and floodplain information can be extracted from DTMs using appropriate terrain analysis (e.g. Nardi *et al.* 2013). The floodplain geomorphic footprint is evident in the topographic datasets, even in significantly dense urban areas, where anthropogenic features (e.g. buildings, streets, levees, weirs and dams) have greatly altered the floodplain morphology and connectivity (Tockner and Stanford 2002, Morrison *et al.* 2018, Nardi *et al.* 2018b). As a result, hydrogeomorphic approaches may rapidly and effectively capture the morphological information associated with riverine water-driven erosion and deposition processes. Hydrogeomorphic floodplain mapping results provide fluvial corridor zoning not specifically linked to flood events, but based on a landscape zoning principle that characterizes fluvial water-dominated environments, supporting multiple hydrological and environmental applications, such as flood-prone area mapping and vulnerability analysis in ungauged regions (Nardi *et al.* 2018b), as well as the analysis of anthropogenic impact on river–floodplain connectivity and ecological processes (Morrison *et al.* 2018, Scheel *et al.* 2018).

Lately, the application of hydrogeomorphic approaches for delineating floodplains has been the subject of an increasing number of research projects as higher resolution DTMs are becoming available. Numerous studies have demonstrated the ability of hydrogeomorphic floodplain mapping techniques and their effectiveness in identifying floodplain regions (e.g. Dodov and Foufoula-Georgiou 2006, Nardi *et al.* 2006, Manfreda *et al.* 2011, 2014, 2015, Sangwan and Merwade 2015, Jafarzadegan and Merwade 2017, Samela *et al.* 2017, Speckhann *et al.* 2017).

However, there are still challenges in hydrogeomorphic floodplain modelling, especially regarding the effects of DTM accuracy and resolution on model results, the potential inaccuracies of terrain analysis algorithms related to artificial depression and flat area issues (e.g. Jenson and Domingue 1988, Garbrecht and Martz 1997a, 1997b, Tarboton and Ames 2001, Jana *et al.* 2007, Nardi *et al.* 2008), and appropriate techniques for calibrating hydrogeomorphic model parameters. Moreover, the selection of a reference floodplain dataset for calibration and validation constitutes a significant challenge for geomorphic floodplain modellers.

The hydrogeomorphic model by Nardi *et al.* (2006, 2018b) proved to be a fast and efficient model for delineating floodplain landscape features. Recent applications of this modelling approach were used to evaluate loss of floodplain connectivity caused by human activity (Nardi *et al.* 2018b) and to quantify the relationship between wetland extension and levee distribution in river basins (Morrison *et al.* 2018, Scheel *et al.* 2018). However, investigations on hydrogeomorphic floodplain modelling performance to changing DTM resolution and stream order hierarchy are missing. In particular, analysis of the floodplain modelling behaviour linked to DTM accuracy, model parameterization and resolution bounding conditions, such as the floodplain initiation in upstream zones, are required to quantitatively evaluate the generalization and consistency of this modelling approach.

To address these challenges, our objectives for this research were to investigate: (1) the influence of DTM resolution and contributing area thresholds on floodplain initiation in river network headwater regions; (2) the impact of river network position and DTM resolution in hydrogeomorphic model parameterization; and (3) differences between hydrogeomorphic model results and standard flood-hazard maps, as well as other simple geomorphic models. Quantitative indices were used to compare the results of a hydrogeomorphic floodplain model to other floodplain mapping simulations. These investigations allowed us to evaluate the importance of proper terrain analysis parameterization for headwater floodplain modelling at varying DTM resolutions. Moreover, the sensitivity of the results to model parameterization with different stream orders was tested against reference floodplain maps. A case study was developed in central Italy, but the proposed performance analysis was also demonstrated for national-scale applications in Hungary, Italy, Spain and the UK.

2 Data and methods

2.1 Study area

The Arno River Basin, central Italy, was selected as a case study site. The Arno basin is the fourth largest catchment in Italy and encompasses approximately

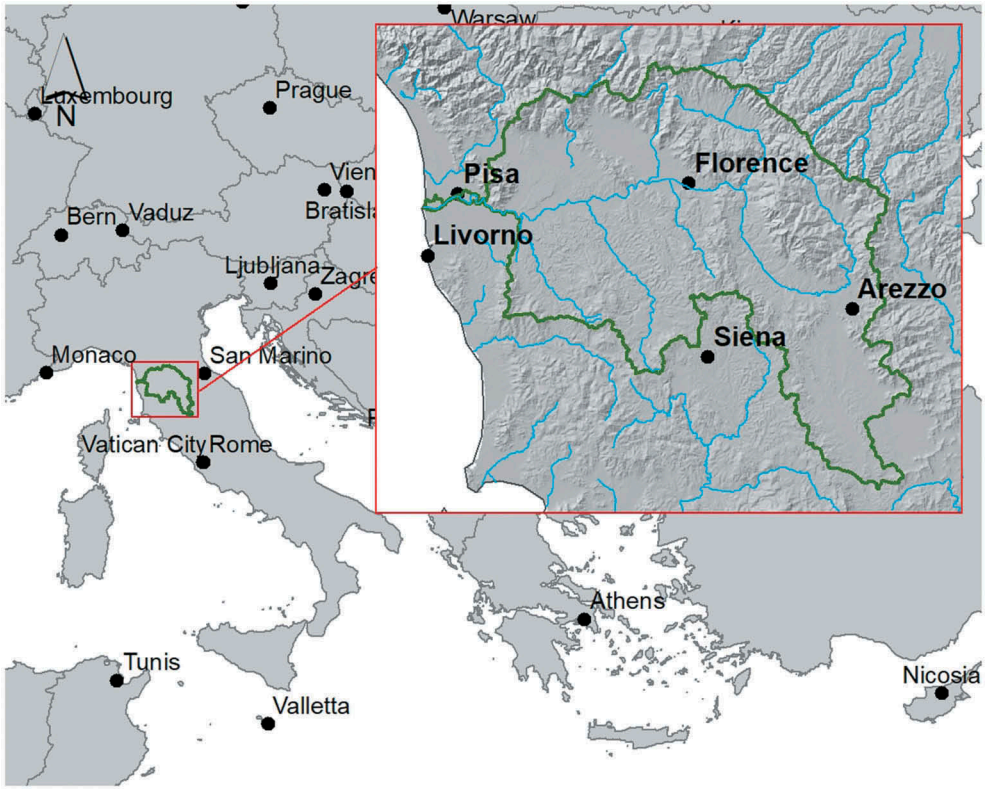

Figure 1. Location map of the study basin: the Arno River.

8500 km^2, primarily in the Tuscany region (Fig. 1). The Arno River drains the Apennine Mountains in central Italy toward the Tyrrhenian Sea, with a maximum elevation difference of 2000 m and average elevation of 345 m a.s.l. The climate of the basin is semi-arid, with a high variability of precipitation during the year. Soil types are mainly brown soil (34%), clay-loam (19%) and alluvial sediment (15%). Approximately 530 km^2 of the basin is urbanized, accounting for 6% of the basin area, and the main land cover types in the basin area are cropland, olive-yards, vineyards and forest (Copernicus Land Service 2012). In Section 3.4, we consider larger domains at the national scale, specifically Hungary, Italy, Spain and UK.

2.2 Hydrogeomorphic floodplain delineation method

This study uses the hydrogeomorphic floodplain mapping algorithm developed by Nardi *et al.* (2006, 2013, 2019) to evaluate the impact of DTM resolution and model parameterization on model performance. This method delineates the floodplain by identifying areas along the fluvial corridor that underlie maximum floodplain flow levels. This model is based on the application of two main steps: (1) terrain analysis routines for river network identification and DTM pre-processing; and (2) application of the hydrological scaling law for estimating maximum flow depths and floodplain mapping.

The river network was identified using a DTM-based approach following standard terrain analysis procedures for pit filling, determining flow direction, estimating flow accumulation (Jenson and Domingue 1988, Grimaldi *et al.* 2004, 2005, Nardi *et al.* 2008) and filtering cells with a contributing area greater than a pre-defined threshold (Tarboton *et al.* 1991, Tarboton and Ames 2001).

The hydraulic geometry equations of Leopold and Maddock (1953), originally developed to relate channel geometry to varying flow discharge, were applied to represent floodplain morphology and flow scaling behaviour (Bhowmik 1984, Nardi *et al.* 2006). The adopted hydrogeomorphic floodplain model uses a power law equation to estimate flow depth as a function of the upstream contributing area (Dodov and Foufoula-Georgiou 2004). Flow depth is calculated as follows:

$$d = aA^b \tag{1}$$

where d is the floodplain flow depth (m), A is the contributing area (m^2), and a (m^{1-2b}) and b (dimensionless) are the power law coefficient and exponent, respectively. The power law parameters

a and b depend on the hydrological, geological, geomorphic and climatic attributes of the river basin (Phillips 2015). Nardi *et al.* (2006) originally assigned values for the power law parameters a and b, implementing a series of steps that relied on estimates of maximum discharge at the basin outlet and hydraulic calculations using floodplain cross-sections extracted from a DTM. This approach is time-consuming and infeasible for DTMs with coarse resolutions, so this study presents an approach that overrides the need for cross-section analyses and maximum outlet peak discharges, adopting a different methodology for assigning the power law parameters. The presented approach, always based on Equation (1), investigates valid ranges of a and b parameters, with varying DTM resolution and scaling conditions, evaluates the performance of the floodplain model with respect to standard flood-hazard maps and compares the performance with other simplified floodplain delineation methods.

2.3 Performance indices and data sources

Numerous quantitative indices are available to evaluate differences between modelled results and reference floodplain data. Standard flood-hazard maps gathered from flood-risk management plans (*Piano di Assetto Idrogeologico*, PAI) were used as reference data. The PAI maps were provided by the Arno River Basin Authority (http://www.adbarno.it) and were developed using hydraulic modelling for a 500-year return period flood. Low-frequency (e.g. 500- or 100-year return period) flood-hazard maps are most appropriate to serve as reference datasets for evaluating the performance of the hydrogeomorphic floodplain zoning, since river corridor morphology is mainly shaped by high-magnitude, low-recurrence events. The performance indices used in this study include an objective measure-to-fit function (F index) (Equation (2); Horrit and Bates 2001), the true positive (TP) index (Equation (3); Samela *et al.* 2017), the sum of false positive (FP) and false negative (FN) rates (Equation (4); Samela *et al.* 2017), and a bias parameter (Equation (5)).

Using the contingency scheme shown in Table 1, the F index is calculated as:

Table 1. Contingency table describing the parameters of the F index from Equation (4).

	Area within reference floodplain	Area outside reference floodplain
Area within modelled floodplain	A	B
Area outside modelled floodplain	C	D

$$F = A/(A + B + C) \tag{2}$$

where A, B and C represent overlapping, over-predicting and under-predicting areas, respectively, of our model results when compared to a reference floodplain map. Values of F range from 0 (poor fit) to 1 (perfect fit).

The TP index (ranging between 0 and 1) quantifies the agreement between the hydrogeomorphic floodplain delineation as compared to the standard flood-hazard map, but without considering the over-prediction parameter B, and is defined as:

$$\mathrm{TP} = A/(A + C) \tag{3}$$

The sum of FP and FN indices (FPN, ranging between 0 and 2) characterizes both over- and under-prediction tendencies of the hydrogeomorphic model. These two indices are inversely proportional to the performance of the model, and the sum of the indices is defined as:

$$\mathrm{FPN} = C/(A + C) + B/(B + D) \tag{4}$$

where D represents the true negative areas (i.e. outside the simulated floodplain and not pertaining to the reference flood-hazard map).

A bias parameter characterizes the general tendency of the hydrogeomorphic model to over-predict or under-predict floodplain areas, and is defined as:

$$\mathrm{Bias} = (A + B)/(A + C) \tag{5}$$

Receiver operating characteristics (ROC) curves (Fawcett 2006) were also considered as auxiliary classifiers.

Four different DTM resolutions were used in the analyses, ranging from 10 m to approx. 250 m. Moreover, the MERIT DTM (Yamazaki *et al.* 2017) was used to validate the model at a larger scale. The MERIT DTM was developed by removing multiple error components (absolute bias, stripe noise, speckle noise and tree height bias) from the existing space-borne DTMs (SRTM3 v2.1 and AW3D-30m v1). The source and resolution of each DTM are shown in Table 2.

2.4 Benchmarking with other simplified methods

Besides comparing the hydrogeomorphic floodplain modelling results to standard flood-hazard maps using Equations (2)–(5) and the ROC curves, we also compared the modelling results to the following simplified floodplain mapping methods:

- Height Above the Nearest Drainage (HAND). The HAND model assigns a constant water depth to the stream network following the

Table 2. Resolution and sources of DTMs used in the hydrogeomorphic floodplain delineation model.

DTM name	Resolution (m)	Source
TINITALY 10m	10	Istituto Nazionale di Geofisica e Vulcanologia (INGV); http://tinitaly.pi.ingv.it/
SRTM 1arc	~30	Shuttle Radar Topography Mission, NASA; https://earthexplorer.usgs.gov/
SRTM 3arc	~90	Shuttle Radar Topography Mission, NASA; https://earthexplorer.usgs.gov/
SRTM 8.3arc	~250	Resampled SRTM 3arc by CGIAR; http://srtm.csi.cgiar.org/
MERIT DEM	~90	http://hydro.iis.u-tokyo.ac.jp/~yamadai/MERIT_DEM/

approach of Nobre *et al.* (2011). The HAND model identifies floodplain areas by considering a constant water depth for stream network cells and flags as floodplain all the cells hydrologically connected to it with an elevation lower than the sum of the stream cell elevation and the assigned water depth.

- Constant hydrological flow distance to the stream network (D). This method identifies floodplain areas by filtering those cells with a hydrological distance from the stream network that is lower than a pre-defined constant value.
- Local slope (S). This method delineates the floodplain based on a simple slope thresholding analysis for identifying flat areas within a river corridor.
- Topographic wetness index (TWI). The TWI method identifies river basin cells as floodplain area using a user-defined TWI threshold. The TWI threshold is related to the frequently saturated area of a river corridor and is calculated as TWI $= \ln(A_c/\tan(S))$, where A_c is the local contributing area per unit contour length and S is the local slope (Beven and Kirkby 1979).

2.5 Floodplain initiation analysis

The definition of contributing area thresholds for extracting river networks is highly dependent on DTM resolution (McMaster 2002). Similarly, the width of simulated floodplains, estimated along the direction perpendicular to the channel flow, is also dependent on DTM resolution. In particular, the floodplain width depends on a minimum number of DTM grid cells that are needed to define the floodplain morphology. A minimum of two DTM cells is imposed here, considering that a floodplain is characterized by at least one cell for the channel and one adjacent cell to define the valley. Using these criteria allows us to take into account cases when one bank of the river centreline is a steep hillslope and the transversal floodplain width can be traced on only one side of the cross-section. This floodplain initiation analysis is performed to avoid representing the floodplain transversal extent in areas where the floodplain width is narrower than the DTM cell size. In this way, the influence of DTM resolution on floodplain mapping in headwater regions is evaluated by plotting the percentage of total floodplain widths larger than two DTM cells with respect to contributing area threshold for the different DTM resolutions.

3 Results

The hydrogeomorphic floodplain delineation model was used to map floodplain areas in the Arno River Basin for each DTM resolution, as well as the floodplains at a national scale in Hungary, Italy, Spain and the UK.

3.1 Effect of contributing area on minimum floodplain width

The contributing area necessary to initiate floodplain delineation was found to be dependent on DTM resolution. Figure 2 shows the percentage of floodplain widths larger than two cells across a range of contributing area thresholds for each DEM resolution. An 80% occurrence limit was used to compare the effect of each DTM resolution. For 10-m and 1-arc (~30 m) DTM resolutions, the relative occurrence of floodplain widths greater than two cells quickly increased as contributing area threshold increased, and 80% of delineated floodplains exceeded a minimum width with contributing areas of 4 and 9 km^2, respectively. At least 80% of floodplains reached a minimum two-cell width after 200 and 300 km^2 for the 3-arc (~90 m) and

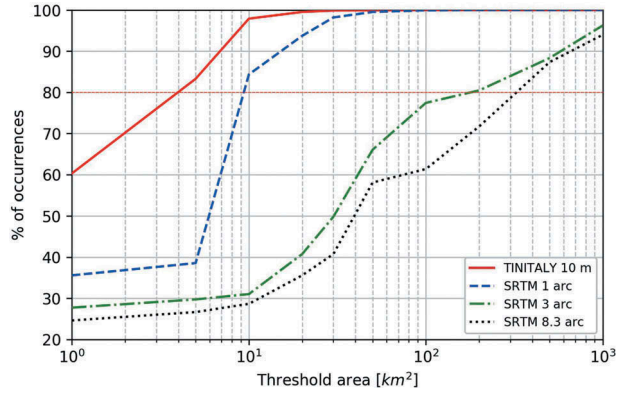

Figure 2. Percentage of occurrence of floodplain width larger than two cells for each DTM with varying contributing area threshold.

8.3-arc (~250 m) DTM resolutions. Contributing areas larger than 1000 km^2 were not evaluated, since they would encompass a large percentage of the entire Arno Basin and limit the river network size.

3.2 Impact of DTM resolution and stream order on parameterization

The PAI flood-hazard maps were used as reference for the performance analysis of the hydrogeomorphic floodplain mapping model. A range of a and b parameters was selected (Table 3) based on values represented in previous studies (Nardi *et al.* 2006, 2013) and used to delineate floodplains in the Arno Basin. The F index values (Equation (2)) were calculated using the PAI flood-hazard maps and the hydrogeomorphic model results. Figure 3 illustrates the F index values associated with combinations of a and b parameter values for each DTM resolution.

Combinations of a and b parameters that resulted in the highest F index value (Equation (2)) were considered optimal parameter values. Linear regressions of optimal log(a) and b values show strong linear correlations for all DTM resolutions (Fig. 3 and Table 4). The semi-log plots of Fig. 3 show a wide range of a and b parameters that produce high F index values. This analysis suggests that consistent values of F index are obtained with varying b parameters with a constant a parameter of 0.01 m^{1-2b}. As a result, considering the strong linear correlation between a and b, further tests investigating the impact of DTM resolution were conducted by holding the a parameter constant, with a value of 0.01 m^{1-2b}, and varying the b parameter according to the respective correlation equation (Table 5). The results show that F indices and optimal b parameter values slightly decrease as DTM resolutions become larger (Table 5).

The impact of river network position on model parameters was evaluated by partitioning model results by the Strahler stream order of network segments. Figure 4 illustrates the F index values associated with combinations of a and b parameter values for the 1-arc DTM and a contributing area threshold of 10 km^2. As shown in Figure 4, these results suggest that higher stream orders (e.g. orders 4 and 5) correspond to lower optimal values of a and b. It is also evident that lower stream orders correspond to lower values of the F index related to the optimal b value. Because lower-order streams typically have narrower floodplain widths compared to higher-order streams, the absolute error of over- or under-prediction is larger in lower-order streams. Table 6 shows the behaviour of the optimum b value for each DTM resolution with a constant a of 0.01 m^{1-2b}. This again demonstrates that higher b values are required for higher-resolution DTMs and lower-order streams.

These results suggest the performance of the hydrogeomorphic floodplain delineation model may be improved by using a and b parameters that are optimal for each stream order in a river network. Table 7 shows that F index values aggregated across the entire Arno Basin increased by approximately 6% when optimal parameters associated with each stream order in the basin were used. The increase in F index results occurred for all DTM resolutions.

Figure 5 illustrates the hydrogeomorphic floodplain delineation model results generated from a 1-arc DTM and optimal combinations of b parameters for each stream order (with a constant at 0.01 m^{1-2b}). The PAI standard flood-hazard map boundaries are shown for comparison.

The hydrogeomorphic model performance was also tested by comparing results from the SRTM 1-arc DTM to flood-hazard maps of various return periods (e.g. 50-, 200- and 500-year recurrence intervals). The results shows that when the a parameter is fixed at 0.01 m^{1-2b}, the b parameter varies considerably for different return periods (Table 8). Also, as the return period increases, the F index also increases. This mean that the model performs best for delineating floodplains generated by higher-magnitude events and is not well suited for delineating floodplain areas generated by low-magnitude events, which do not inundate entire river valleys. Also, the lower F index value calculated for the 50-year return period is partially due to floodplain areas being constrained by levees in the lower portion of the basin.

3.3 Comparison to other geomorphic methods

Numerous studies have generally compared floodplain delineation methods (e.g. Noman *et al.* 2001, Samela *et al.* 2015, 2017, Rathjens *et al.* 2016). However, we wanted to compare our hydrogeomorphic floodplain model to other well-known geographic methods to specifically assess its performance. Results from the hydrogeomorphic delineation model were compared to other floodplain geomorphic modelling using Equations (2)–(5). Performance indices for each model (described in Section 2.3) were calculated using 1-arc DTM resolution and the PAI flood-hazard maps

Table 3. Value range of the power law parameters a and b used in the performance analysis.

Power law parameter	Range of values	Interval
a (m^{1-2b})	0.0002–1	Variable (0.002–0.5)
b (-)	0.20–0.60	0.01

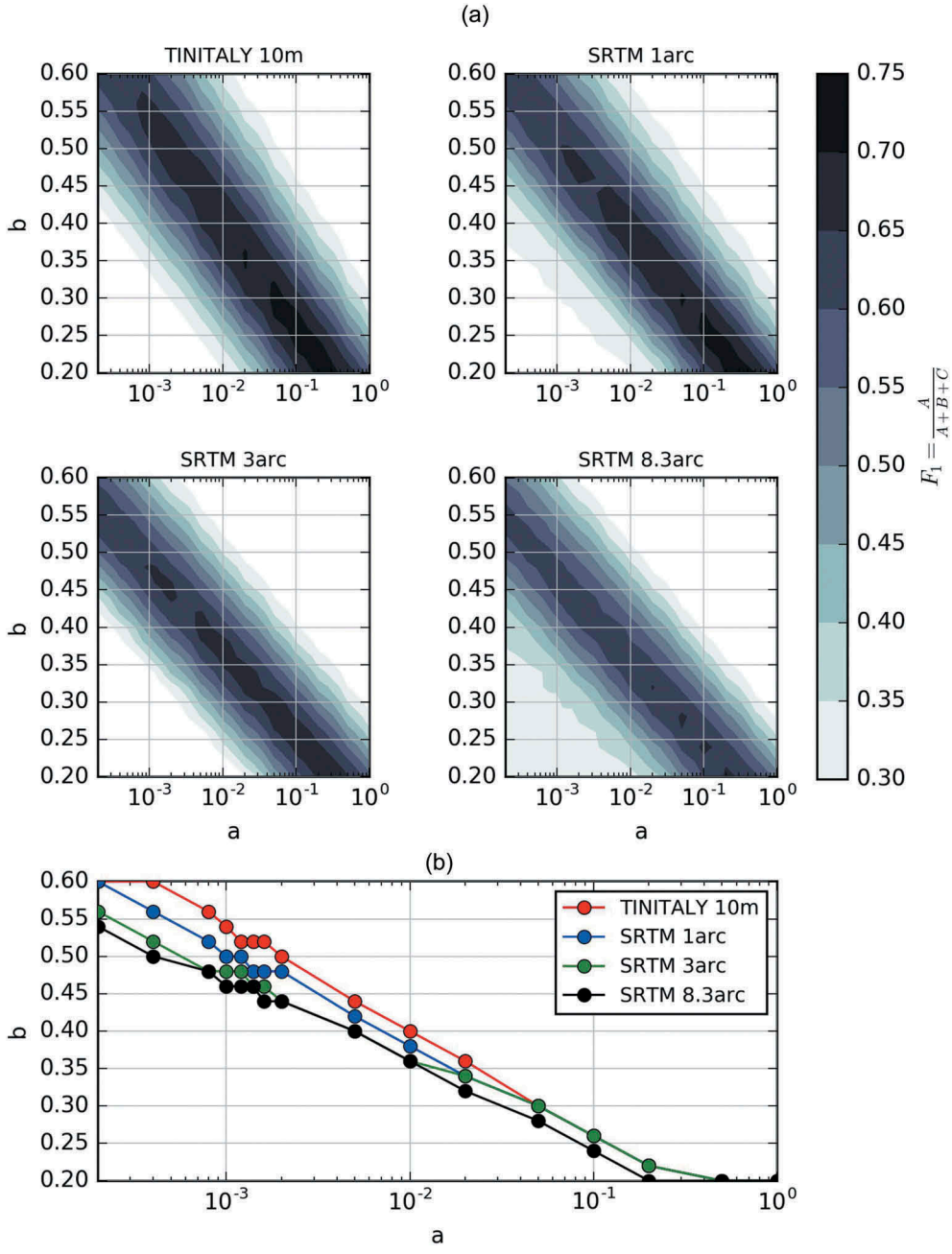

Figure 3. (a) Contour plots of the *F* index for different DTMs representing the performance of optimal combinations of parameters *a* and *b* (Equation (1)). (b) Optimal combinations of *a* and *b* parameters for each DTM.

Table 4. Results of linear correlation between the optimal log (*a*) and *b* values for each DEM ($b(a) = i + s \log(a)$).

DEM	Slope, *s*	Intercept, *i*	R^2	Standard error
TINITALY 10m	−0.055	0.1565	0.985	0.0018
SRTM 1arc	−0.05	0.1596	0.988	0.0015
SRTM 3arc	−0.045	0.1679	0.990	0.0012
SRTM 8.3arc	−0.044	0.1599	0.982	0.0016

Table 5. Optimal values of *b* and *F* index for the selected DEMs, corresponding to *a* equal to 0.01 m^{1-2b}

DTM	Optimal *b*	*F* index
TINITALY 10m	0.4	0.696
SRTM 1arc	0.38	0.686
SRTM 3arc	0.37	0.675
SRTM 8.3arc	0.36	0.649

as reference data. Table 9 and Figure 6 show the performance of the hydrogeomorphic floodplain method compared to the other geomorphic models. The results shown in Table 9 correspond to the parameters associated with peak *F* index values. The results from the hydrogeomorphic floodplain model improved *F* index values by 40–50% compared to the other methods. In addition, the FPN and Bias values for the

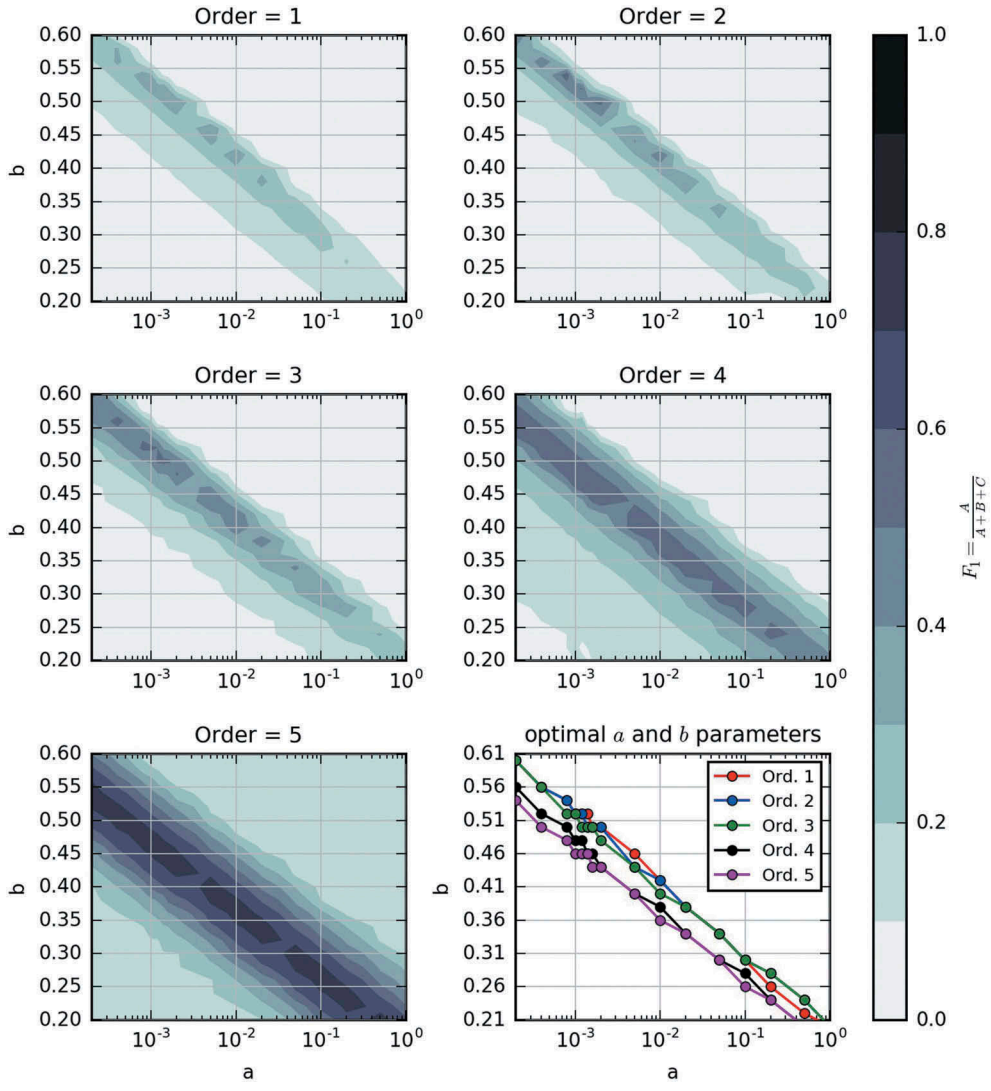

Figure 4. Contour plots of the *F* index for SRTM 1-arc DTMs and optimal combinations of *a* and *b* parameters with varying stream order.

Table 6. Optimal values of *b* for each DTM resolution and stream order, corresponding to *a* equal to 0.01 m^{1-2b}.

	DTM			
Stream order	TINITALY 10m	SRTM 1arc	SRTM 3arc	SRTM 8.3arc
1	0.44	0.43	0.42	0.41
2	0.43	0.42	0.36	0.32
3	0.42	0.4	0.34	0.33
4	0.4	0.38	–	–
5	0.39	0.36	–	–

Table 7. Values of *F* index obtained using a single optimal *b* parameter, and optimal *b* that varies by stream order.

	F index	
DTM	Single optimal *b*	Optimal *b* for each stream order
TINITALY 10m	0.696	0.7184
SRTM 1arc	0.686	0.7143
SRTM 3arc	0.675	0.709
SRTM 8.3arc	0.649	0.677

hydrogeomorphic method were the lowest among all the models, given the optimal parameters for each model. The ROC curves were considered for the available TP and FP rates using the limited range of values of the parameters of each geomorphic model. Figure 8 shows the performance of the selected hydrogeomorphic floodplain model with respect to the other geomorphic methods in terms of ROC curves, even when the elevation difference stayed in different ranges of FP rates and could not be visually compared. In this case, the total area under the ROC curve (AUC; Fawcett 2006) cannot be calculated because of the limited ranges of TP and FP rates. A visual comparison among the different geomorphic methods is illustrated in Figure 7.

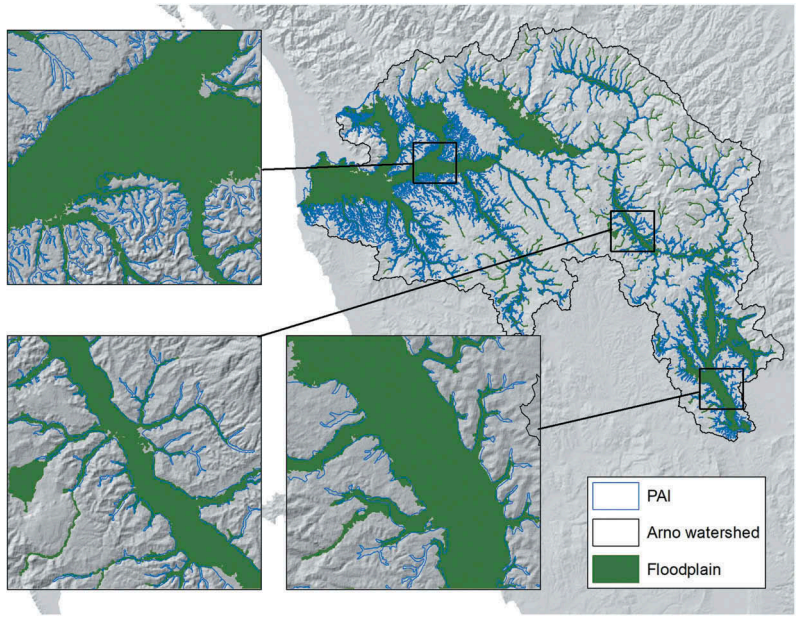

Figure 5. Floodplain mapping results for the Arno River basin using 1-arc DTM resolution.

Table 8. Optimal power law b parameters and relative F index for different return periods adopting the SRTM 1arc DEM and the power law a parameter equal to 0.01 m^{1-2b}.

	Return period (years)		
	50	200	500
Optimal b parameter	0.28	0.34	0.38
Maximum F index	0.288	0.61	0.686

3.4 Evaluating the hydrogeomorphic model in larger-scale applications

The hydrogeomorphic floodplain model was tested in larger-scale areas characterized by different climate and morphology using the MERIT-DTM (3-s resolution, Yamazaki *et al.* 2017) and a threshold area for stream initiation of 100 km^2. Country-scale applications of the model were performed for Hungary, Italy, Spain and the UK. In these countries, standard flood-hazard maps (500-year return period) are available as reference data (Table 10). To apply the hydrogeomorphic floodplain model for the Hungarian region, the headwater region of the Danube Basin in Italy, Germany, Czech Republic, Austria, Poland, and the Slovak Republic was also considered. The comparison between the standard flood-hazard maps and the floodplain extent was performed by fixing the a parameter to 0.01 m^{1-2b} and varying the b parameter in the same range considered for the previous sensitivity analysis (Table 3). Box plots (Fig. 9) show a relatively low variance in the optimal b parameter, especially in higher-order streams, where morphometric parameters, such as basin and stream slopes, are less variable than in upstream portions of the basins. The median values of the b parameter tend to decrease with increasing stream order, as previously confirmed in the Arno Basin (Fig. 4). For the Spain and UK case studies, there is a slight increase in median b values at the largest-order streams, but this behaviour is not considered statistically significant since there is only one stream segment for these orders.

4 Discussion

In this work, a hydrogeomorphic floodplain model was applied and its performance evaluated with varying DTM resolution and stream order. The performance

Table 9. Summary of the performance index analysis comparing the hydrogeomorphic floodplain model with four other simplified geomorphic models. HAND: Height Above the Nearest Drainage model; D: constant hydrological flow distance to the stream network; S: local slope; TWI: topographic wetness index; TP: true positive; FPN: false positive plus false negative.

Model	Threshold parameter	Threshold value	F index	TP	FPN	Bias
Hydrogeomorphic	Exponent of the Leopold law, b	0.38	0.686	0.806	0.246	0.985
HAND	Stream water depth (m)	5.7	0.296	0.963	0.688	3.215
D	Stream distance (m)	1585	0.29	0.607	0.709	1.698
S	Slope value (%)	3	0.634	0.826	0.262	1.129
TWI	Index value (-)	6.5	0.289	0.645	0.71	1.876

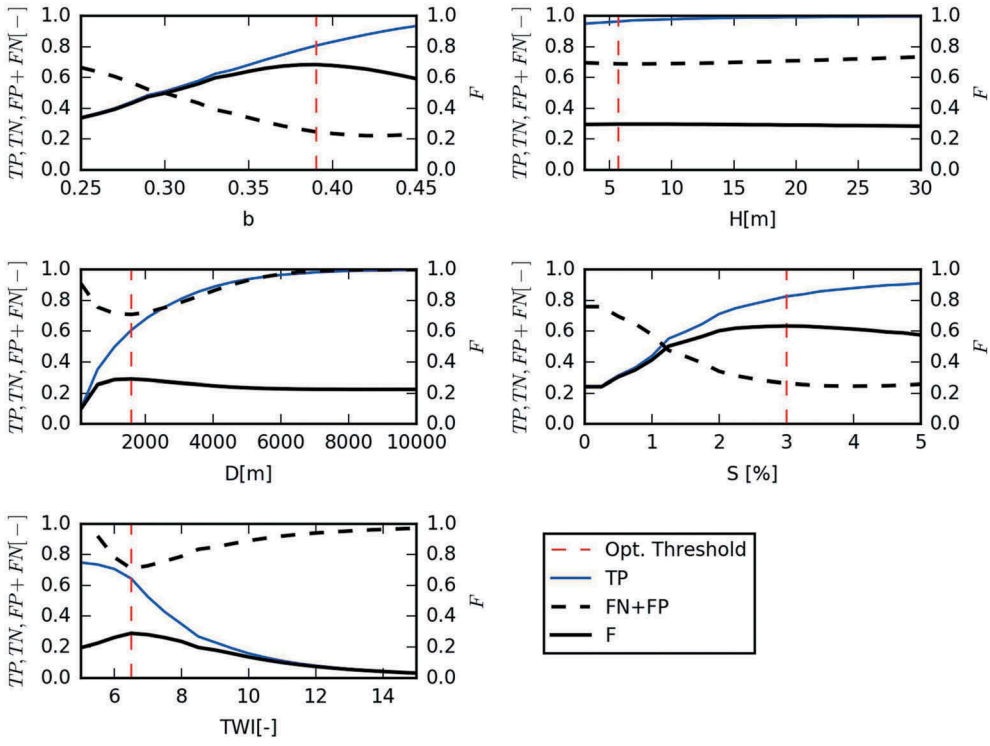

Figure 6. Benchmarking analysis of the floodplain model with respect to other geomorphic algorithms (TP: true positives, FN+FP: sum of false positives and false negatives, *F* index).

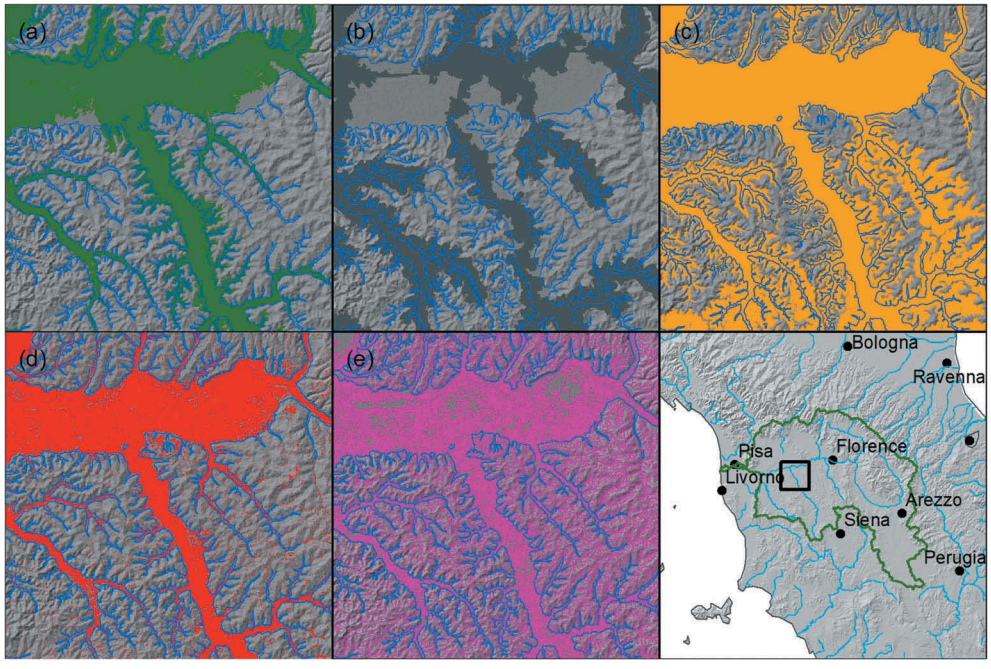

Figure 7. (a) Section of the Arno River basin floodplain – see inset in bottom right map – and visual comparison of the hydrogeomorphic model with respect to: (b) HAND; (c) constant hydrological flow distance, D; (d) local slope, S; and (e) TWI. The PAI 500-year flood-hazard zoning is indicated in blue.

of the model was compared to standard flood-hazard maps with the aim of understanding and identifying model behaviour and optimal parameterization for floodplain mapping.

The results demonstrate that DTM resolution influences the behaviour of the hydrogeomorphic floodplain mapping model. This is expected, considering that the adopted geomorphic mapping principle enforces the

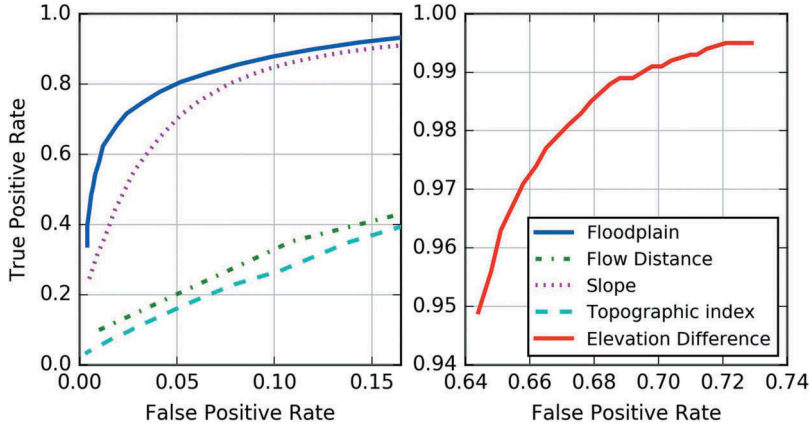

Figure 8. Partial ROC curves of the geomorphic algorithms in the available true and false positive rate ranges.

Table 10. List of the countries and the related standard flood-hazard maps adopted for testing the floodplain delineation model.

	Standard flood-hazard maps		
Country	Return period (years)	Provider	Source
Hungary	1000	Ministerio para la Transición Ecológica	http://www.vizugy.hu
Italy	500	Italian District Authorities	Eight websites (e.g. http://www.adbpo.it/download/PAI_FasceFluviali/
Spain	500	Vízügyi honlap	http://www.mapama.gob.es/es/cartografia-y-sig/ide/descargas/agua
UK	1000	data.gov.uk	https://data.gov.uk/dataset/risk-of-flooding-from-rivers-and-sea1

concept that floodplain features are identifiable from DTMs as topographic information linked to flooding processes that shape fluvial environments. Generally, the optimal b parameter in the power law equation used to estimate flood depth increased as DTM resolution became finer. This is likely because finer-resolution DTMs capture more channel morphology details, thus requiring slightly higher b parameters to estimate a given flood depth compared to a lower-resolution DTM. The results also demonstrate that the model calibration can be restricted to one parameter because of the strong linear dependency of the a and b parameters. For instance, if a value for the a parameter included in the analysed range is selected, a range of b values can be

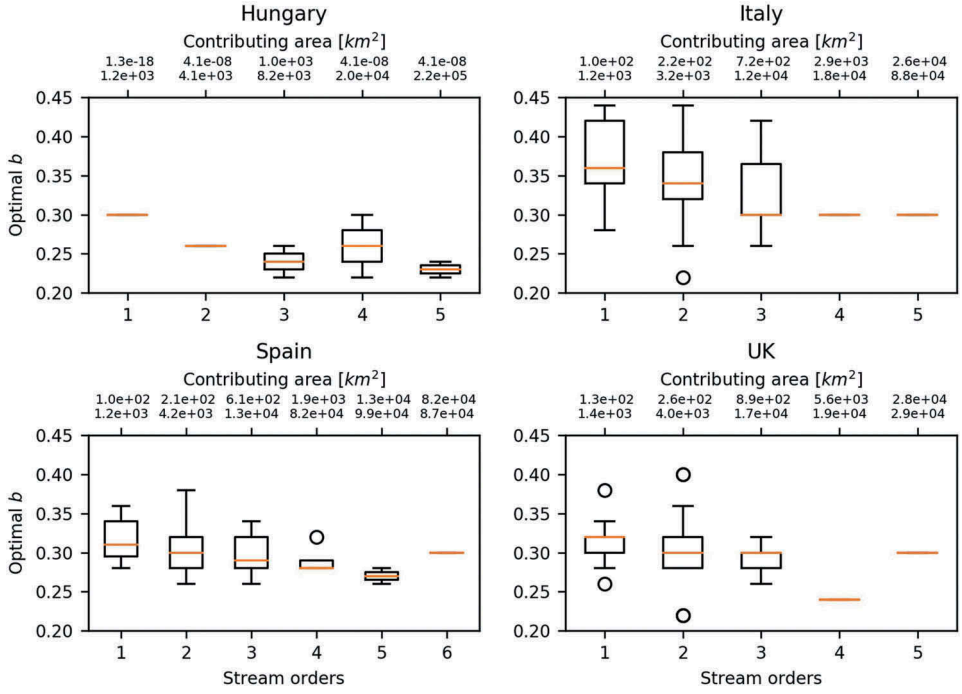

Figure 9. Box plot of the optimal b parameters varying the stream order for four countries.

tested until the expected results are reached. The differences among optimal combinations of parameters for different DTM resolutions becomes less relevant for higher *a* values (e.g. Fig. 3). It is important to note that the *F* index analysis presented in this study is affected by the heterogeneous spatial availability of PAI flood maps, which may not cover an entire catchment, especially for upstream areas.

River network hierarchy was also shown to influence optimal scaling parameter values. This is likely a reflection of fluvial geomorphic attribute gradients associated with low- to high-order river systems (e.g. Thorp *et al.* 2008).

In higher-order streams (e.g. stream orders 4–5), typically characterized by U-shaped valleys and more urbanization, a narrower range of optimal *b* values was discovered. In these regions, larger *b* values corresponded to significant overestimation of flood-prone areas. The challenge of finding optimal parameters for stream order 4 possibly corresponds to the transition zone between uplands and downstream areas.

Although this study used flood-hazard maps to evaluate model performance, the results should not be used to suggest that hydrogeomorphic floodplain modelling is a surrogate for the lack of flood-hazard maps. Nonetheless, the performance of the model demonstrates the consistency of hydrogeomorphic floodplain mapping across multiple geomorphic settings and with varying DTM resolution. The scope of analyses in this study, ranging from floodplain initiation thresholds with varying DTM resolutions to overall impacts of river network hierarchy, supports the validity of the theoretical formalism of the hydrogeomorphic mapping algorithm to extract river valley information from DTMs. The presented floodplain mapping algorithm serves as a geomorphic tool able to characterize the sign of past fluvial hydrological and geomorphic processes.

This study can serve as a potential guide for identifying reasonable ranges of parameter values at basin to global scales for given DTM resolutions and range of stream orders. In fact, the results of the validation analysis performed for Hungary, Italy, Spain and the UK show a relatively low variance of the optimal parameters, mostly for higher stream orders.

5 Conclusions

This study systematically evaluated the impact of DTM resolution and model parameterization on the performance of a hydrogeomorphic floodplain mapping algorithm. The mapping algorithm was evaluated in the Arno River study basin using four different DTMs, with resolutions ranging between 10 and 250 m. The contributing area threshold analysis for floodplain initiation and the sensitivity analysis of power law parameters *a* and *b* with varying DTM resolution was developed in quantitative terms. The results show a dependency between the optimal power law parameters and DTM resolution, with larger parameter values required to reach optimal consistency with flood-hazard maps as DTM resolution increased. Floodplain mapping performance was also found to depend on stream order, and the best performance occurred when comparing modelling results to flood-hazard maps of lowest return periods.

Author contribution

A.A. and F.N. conceived the research project, carried out the hydrogeomorphic model development and application and drafted the first version of the manuscript. A.A. developed the data gathering and hydrogeomorphic floodplain modelling activities and produced all tables and figures presented in the manuscript. F.C. and R.M. supported the research supervision and implementation and contributed to the interpretation of the results, providing critical feedback to A.A. and F.N. in shaping the research, analysis and manuscript preparation. R.M. and F.N. significantly supported A. A. in writing of the final version of the manuscript.

Disclosure statement

No potential conflict of interest was reported by the authors.

ORCID

A. Annis http://orcid.org/0000-0001-6162-4691
F. Nardi http://orcid.org/0000-0002-6562-3159
R. R. Morrison http://orcid.org/0000-0002-8612-1684
F. Castelli http://orcid.org/0000-0003-0304-0289

References

Alfieri, L., *et al.*, 2014. Advances in pan-European flood hazard mapping. *Hydrological Processes*, 28 (13), 4067–4407. doi:10.1002/hyp.v28.13

Alfieri, L., *et al.*, 2017. Global projections of river flood risk in a warmer world. *Earth's Future*, 5 (2), 171–182. doi:10.1002/2016EF000485

Baynes, E.R., *et al.*, 2015. Erosion during extreme flood events dominates Holocene canyon evolution in northeast Iceland. *Proceedings of the National Academy of Sciences*, 112 (8), 2355–2360. doi:10.1073/pnas.1415443112

Beven, K.J. and Kirkby, M.J., 1979. A physically based, variable contributing area model of basin hydrology. *Hydrological Sciences Journal*, 24 (1), 43–69. doi:10.1080/02626667909491834

Bhowmik, N.G., 1984. Hydraulic geometry of floodplains. *Journal of Hydrology*, 68 (1–4), 369–401. doi:10.1016/0022-1694(84)90221-X

Bradshaw, C.J., *et al*., 2007. Global evidence that deforestation amplifies flood risk and severity in the developing world. *Global Change Biology*, 13 (11), 2379–2395. doi:10.1111/j.1365-2486.2007.01446.x

Copernicus Land Service, 2012. *Pan European component: corine land cover* [online]. Copernicus Programme. Available from: https://land.copernicus.eu/pan-european/corine-land-cover/clc-2012 Accessed 11 November 2018

Di Baldassarre, G., *et al*., 2010. Flood fatalities in Africa: from diagnosis to mitigation. *Geophysical Research Letters*, 37 (22), 1–5. doi:10.1029/2010GL045467

Dietrich, W.E. and Perron, J.T., 2006. The search for a topographic signature of life. *Nature*, 439 (7075), 411. doi:10.1038/nature04340

Dodov, B.A. and Foufoula-Georgiou, D., 2006. Floodplain morphometry extraction from a high-resolution digital elevation model: a simple algorithm for regional analysis studies. *IEEE Geoscience and Remote Sensing Letters*, 3 (3), 410–413. doi:10.1109/LGRS.2006.874161

Dodov, B.A. and Foufoula-Georgiou, E., 2004. Generalized hydraulic geometry: derivation based on a multiscaling formalism. *Water Resources Research*, 4 (6), 1–22.

Dottori, F., *et al*., 2016a. Development and evaluation of a framework for global flood hazard mapping. *Advances in Water Resources*, 94, 87–102. doi:10.1016/j.advwatres.2016.05.002

Dottori, F., *et al*., 2016b. *Flood hazard map of the World - 100-year return period* [online]. European Commission, Joint Research Centre (JRC), Available from: http://data.europa.eu/89h/jrc-floods-floodmapgl_rp100y-tif Accessed 11 November 2018

EM-DAT (Emergency Events Database), 2013. *The OFDA/CRED international disaster database*. Belgium: Ottignies-Louvain-la-Neuve: Université catholique de Louvain.

Fawcett, T., 2006. An introduction to ROC analysis. *Pattern Recognition Letters*, 27 (8), 861–874. doi:10.1016/j.patrec.2005.10.010

Garbrecht, J. and Martz, L.W., 1997a. The assignment of drainage direction over flat surfaces in raster digital elevation models. *Journal of Hydrology*, 193, 204–213. doi:10.1016/S0022-1694(96)03138-1

Garbrecht, J. and Martz, L.W., 1997b. *TOPAZ, An automated digital landscape analysis tool for topographic evaluation, drainage identification, watershed segmentation and subcatchment parameterization. TOPAZ User Manual*. El Reno, OK: US Department of Agriculture - Agricultural Research Service, Grazinglands Research Laboratory.

Grimaldi, S., Teles, V., and Bras, R.L., 2004. Sensitivity of a physically based method for terrain interpolation to initial conditions and its conditioning on stream location. *Earth Surface Processes and Landforms*, 29 (5), 587–597. doi:10.1002/(ISSN)1096-9837

Grimaldi, S., Teles, V., and Bras, R.L., 2005. Preserving first and second moments of the slope area relationship during the interpolation of digital elevation models. *Advances in Water Resources*, 28 (6), 583–588. doi:10.1016/j.advwatres.2004.11.014

Horritt, M.S., and Bates, P. D., 2001. Effects of spatial resolution on a raster based model of flood flow. *Journal of Hydrology*, 253 (1–4), 239–249. doi:10.1016/S0022-1694(01)00490-5

Ignacio, J.A.F., *et al*., 2015. Assessing the effectiveness of a social vulnerability index in predicting heterogeneity in the impacts of natural hazards: case study of the Tropical Storm Washi flood in the Philippines. *Vienna Yearbook of Population Research*, 13, 91–129.

Jafarzadegan, K. and Merwade, V.A., 2017. DEM-based approach for large-scale floodplain mapping in ungauged watersheds. *Journal of Hydrology*, 550, 650–662. doi:10.1016/j.jhydrol.2017.04.053

Jana, R., *et al*., 2007. An enhanced technique in construction of the discrete drainage network from low-resolution spatial database. *Computers and Geosciences*, 33 (6), 717–727. doi:10.1016/j.cageo.2006.06.002

Jenson, S.K. and Domingue, J.O., 1988. Extracting topographic structure from digital elevation data for geographic information system analysis. *Photogrammetric Engineering and Remote Sensing*, 58 (11), 1593–1600.

Leopold, L.B. and Maddock, T., 1953. *The hydraulic geometry of stream channels and some physiographic implications*. Washington, DC: US Government Printing Office.

Manfreda, S., *et al*., 2014. Investigation on the use of geomorphic approaches for the delineation of flood prone. *Journal of Hydrology*, 517, 863–876. doi:10.1016/j.jhydrol.2014.06.009

Manfreda, S., *et al*., 2015. Flood-prone areas assessment using linear binary classifiers based on flood maps obtained from 1D and 2D hydraulic models. *Natural Hazards*, 79 (2), 735–754. doi:10.1007/s11069-015-1869-5

Manfreda, S., Di Leo, M., and Sole, A., 2011. Detection of flood prone areas using digital elevation models. *Journal of Hydrologic Engineering*, 16 (10), 781–790. doi:10.1061/(ASCE)HE.1943-5584.0000367

McMaster, K.J., 2002. Effects of digital elevation model resolution on derived stream network positions. *Water Resources Research*, 38 (4), 13-1-13-8. doi:10.1029/2000WR000150

Montanari, A., *et al*., 2013. Panta Rhei—everything flows: change in hydrology and society—the IAHS scientific decade 2013–2022. *Hydrological Sciences Journal*, 58 (6), 1256–1275. doi:10.1080/02626667.2013.809088

Morrison, R.R., *et al*., 2018. Spatial relationships of levees and wetland systems within floodplains of the Wabash Basin, USA. *JAWRA Journal of the American Water Resources Association*, 54 (4), 934–948. doi:10.1111/jawr.2018.54.issue-4

Nardi, F., *et al*., 2008. Hydrogeomorphic properties of simulated drainage patterns using digital elevation models: the flat area issue. *Hydrological Sciences Journal*, 53 (6), 1176–1193. doi:10.1623/hysj.53.6.1176

Nardi, F., *et al*., 2013. Comparing a large-scale DEM-based floodplain delineation algorithm with standard flood maps: the tiber river basin case study. *Irrigation and Drainage*, 62 (S2), 11–19. doi:10.1002/ird.v62.S2

Nardi, F., *et al*., 2018b. Hydrologic scaling for hydrogeomorphic floodplain mapping: insights into human-induced floodplain disconnectivity. *River Research and Applications*, 34 (7), 675–685. doi:10.1002/rra.v34.7

Nardi, F., *et al*., 2019. GFPLAIN250m a global high-resolution dataset of earth's floodplains. *Scientific Data*, 6, 180309.

Nardi, F., Annis, A., and Biscarini, C., 2018a. On the impact of urbanization on flood hydrology of small ungauged basins: the case study of the Tiber river tributary network within

the city of Rome. *Journal of Flood Risk Management*, 11, S594–S603. doi:10.1111/jfr3.2018.11.issue-S2

Nardi, F., Vivoni, E.R., and Grimaldi, S., 2006. Investigating a floodplain scaling relation using a hydrogeomorphic delineation method. *Water Resources Research*, 42 (9), 1–15. doi:10.1029/2005WR004155

Nobre, A.D., *et al.*, 2011. Height Above the Nearest Drainage–a hydrologically relevant new terrain model. *Journal of Hydrology*, 404 (1), 13–29. doi:10.1016/j.jhydrol.2011.03.051

Noman, N.S., Nelson, E.J., and Zundel, A.K., 2001. Review of automated floodplain delineation from digital terrain models. *Journal of Water Resources Planning and Management*, 127 (6), 394–402. doi:10.1061/(ASCE)0733-9496(2001)127:6(394)

Phillips, J.D., 2015. Hydrologic and geomorphic flow thresholds in the Lower Brazos River, Texas, USA. *Hydrological Sciences Journal*, 60 (9), 1631–1648. doi:10.1080/02626667.2014.943670

Rathjens, H., et al., 2016. Delineating floodplain and upland areas for hydrologic models: a comparison of methods. *Hydrological Processes*, 30 (23), 4367–4383. doi:10.1002/hyp.10918

Samela, C., *et al.*, 2015. DEM-based approaches for the delineation of flood-prone areas in an ungauged basin in Africa. *Journal of Hydrologic Engineering*, 21 (2), 06015010. doi:10.1061/(ASCE)HE.1943-5584.0001272

Samela, C., Troy, T.J., and Manfreda, S., 2017. Geomorphic classifiers for food-prone areas delineation for data-scarce environments. *Advances in Water Resources*, 102, 13–28. doi:10.1016/j.advwatres.2017.01.007

Sampson, C.C., *et al.*, 2015. A high-resolution global flood hazard model. *Water Resources Research*, 51 (9), 7358–7381. doi:10.1002/2015WR016954

Sangwan, N. and Merwade, V., 2015. A faster and economical approach to floodplain mapping using soil information. *JAWRA Journal of the American Water Resources Association*, 51 (5), 1286–1304. doi:10.1111/1752-1688.12306

Scheel, K., *et al.*, 2018. Understanding the large-scale influence of levees on floodplain connectivity using a hydrogeomorphic approach. *Journal of the American Water Resources Association*. doi:10.1111/1752-1688.12717

Speckhann, G.A., *et al.*, 2017. Flood hazard mapping in Southern Brazil: a combination of flow frequency analysis and the HAND model. *Hydrological Sciences Journal*, 63 (1), 87–100. doi:10.1080/02626667.2017.1409896

Tarboton, D.G. and Ames, D.P., 2001. Advances in the mapping of flow networks from digital elevation data. *In*: *Bridging the gap: meeting the world's water and environmental resources challenges*, 20–24 May 2001. Orlando, Reston: American Society of Civil Engineers, 1–10.

Tarboton, D.G., Bras, R.L., and Rodriguez-Iturbe, I., 1991. On the extraction of channel networks from digital elevation data. *Hydrological Processes*, 5 (1), 81–100. doi:10.1002/(ISSN)1099-1085

Thorp, J.H., Thoms, M.C., and Delong, M.D., 2008. *The river ecosystem synthesis*. Oxford: Academy Press.

Tockner, K. and Stanford, J.A., 2002. Riverine flood plains: present state and future trends. *Environmental Conservation*, 29, 308–330. doi:10.1017/S037689290200022X

Ward, P.J., *et al.*, 2015. Usefulness and limitations of global flood risk models. *Nature Climate Change*, 5 (8), 712. doi:10.1038/nclimate2742

Wing, O.E., *et al.*, 2017. Validation of a 30 m resolution flood hazard model of the conterminous United States. *Water Resources Research*, 53 (9), 7968–7986. doi:10.1002/2017WR020917

Yamazaki, D., *et al.*, 2017. A high-accuracy map of global terrain elevations. *Geophysical Research Letters*, 44 (11), 5844–5853. doi:10.1002/2017GL072874